Monte Carlo simulation of the charge distribution induced by a high-energy electron beam in an insulating target

2002 J. Phys.: Condens. Matter 14 231

(http://iopscience.iop.org/0953-8984/14/2/310)

INSTITUTE OF PHYSICS PUBLISHING JOURNAL OF PHYSICS: CONDENSED MATTER

J. Phys.: Condens. Matter **14** (2002) 231–247 PII: S0953-8984(02)27073-3

Monte Carlo simulation of the charge distribution induced by a high-energy electron beam in an insulating target

R Renoud, F Mady and J-P Ganachaud

LPIO (EA 3254)/LPST, Faculté des Sciences et des Techniques, Université de Nantes, 2 rue de la Houssinière, BP 92208, 44322 Nantes Cédex 03, France

E-mail: raphael.renoud@physique.univ-nantes.fr

Received 27 July 2001, in final form 14 September 2001
Published 13 December 2001
Online at stacks.iop.org/JPhysCM/14/231

Abstract

We have developed a simulation model of the implantation of a negative charge into an insulating target by a fixed and well-focused high-energy electron beam. We are particularly interested in the evolution of the distribution of the charges trapped during the bombardment.

Our simulation is based on a Monte Carlo method permitting us to account for the various electron–insulator interactions. The charge carriers, unless they are emitted into vacuum, are followed until they have lost most of their kinetic energy. After that, they drift along the internal electric field lines before getting trapped. The field generated by these trapped charges is calculated self-consistently by solving the appropriate Poisson equation.

When the trapping site density is sufficiently high, the dynamics of the charge is principally governed by the self-regulation of the total secondary emission yield. The total number of implanted charges is therefore limited and a quasi-stationary regime arises.

The charge distribution builds up, forming a negative semi-ellipsoidal shell whose extent is directly related to the maximum penetration of the primary electrons. The internal region corresponds to a mixing zone with a weak positive mean charge. This characteristic distribution appears at all the primary beam energies considered.

On the other hand, when the trapping site density is too low, the whole region under the beam is saturated and the mixing zone is completely occupied by electrons before the self-regulation of the total secondary yield acts.

1. Introduction

Charge accumulation in an insulator due to the application of an external stress (force, temperature gradient, electrical field, particle irradiation, ...) plays a leading role in the aging

and breakdown of these materials [1,2]. These phenomena give rise to severe limitations when the insulators are used in industrial applications (electronics, electric wires, aeronautics, ...). The charge represents also a major difficulty in quantitative analysis experiments which use an electron beam or more simply for electron microscopy imaging [3].

The importance of the defects (in a broad sense) in charge-building physics in insulators seems today well established. From a microscopic point of view [4, 5], the trapping of excess charges on these defects gives rise to polarization effects in the medium, allowing the storage of an important electromechanical energy. This latter can be released when relaxation (detrapping) takes place. Breakdown may then follow when relaxation occurs abruptly. In the hope of reducing the degradations caused by the application of a stress, it is thus necessary to analyse not only the physical processes which take place, but also the nature and the repartitioning of the defects which play a role in these processes (characterization of the sample).

During the last 20 years, many characterization techniques have appeared (see for instance [6] for a review of the methods developed). The use of an electron beam is particularly interesting because it permits one to control the injection of the charge inside the target. However, it remains difficult to extract from such measurements what is due to charge transport, to trapping or to relaxation. Thus the interpretation of the results requires one to have access to additional information such as the spatial distribution of the implanted charges or the topography of the electric field and of the potential that they produce.

The use of computer simulations *a priori* allows one to solve this kind of problem. By using the Monte Carlo method, Kotera and Suga [7] calculated the trajectories of electrons injected in the presence of an electric field generated by a negative charge distribution assumed to have been previously implanted in the target (frozen-in charge distribution). In particular, they showed the relation between the value of the pre-implanted dose and the slowing-down effect that it exerts on the primary beam. This dependence explains the reduction of the effective energy of the beam and consequently that of the interaction volume compared to the case of an uncharged sample. The calculations are nevertheless performed for a static charge distribution for which no dynamic time evolution is accounted for.

This step has been achieved by Vicario and co-workers [8, 9]. Their simulation is based on the use of the so-called 'simple diffusion' method. After they have lost most of their kinetic energy, the charge carriers get trapped and contribute to the internal electrostatic field which is self-consistently calculated. These authors were thus able to give the time evolution of the implanted charge. Nevertheless, their description of the elementary processes remains sometimes a little rough. In particular, to treat the secondary-electron emission they use '*a priori*' models where the consequences of the presence of an electric field are not clearly included.

During the last few years, insulator charging simulations have been performed for instance in the context of electron beam lithography where the charge effects disturb the electron beam and cause pattern displacement errors [10, 11]. This is also true for x-ray microanalysis [12] where the depth distribution function for characteristic x-ray production (the so-called $\phi(\rho z)$) may be distorted, rendering the quantitative interpretation particularly difficult.

In this work, we have tried to model the implantation of a negative charge in an insulating sample by describing the complete history of the electrons and of the holes excited during the inelastic collisions. When they have lost their kinetic energy, the charge carriers drift along the electric field lines until they stabilize on a trapping site. Thus they contribute to the electrostatic field, which is calculated self-consistently.

After briefly recalling our model, we shall comment on the results we have obtained by the simulation of the implantation of a dose of a few picocoulombs in an amorphous SiO_2

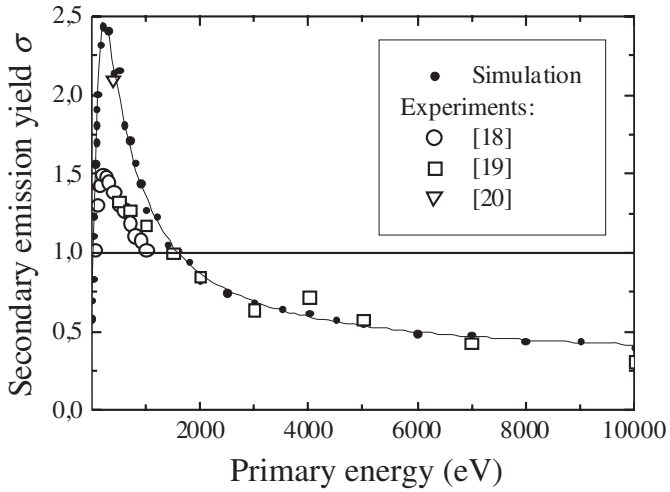

Figure 1. Total secondary-electron emission yield σ as a function of the primary energy E_p. Comparison of the values obtained by simulation with the experimental data of [18–20]. The simulated curve has been obtained by inhibiting the charge effects (standard emission curve).

target. We are primarily interested in the shape of the charge distribution obtained and in its evolution during the electron bombardment. The influence of the primary energy and of the density of trapping sites on the implanted charge behaviour will then be discussed.

2. Review of the electron–insulator interaction model

During the bombardment of an insulating target by an electron beam, the primary electrons and the electron–hole pairs excited via the inelastic collisions have their trajectory and their energy strongly influenced by the internal electric field which progressively develops in the sample. To describe the history of these charge carriers, we use a Monte Carlo simulation program.

In a first stage of its history, an injected electron follows the classical collision scheme (elastic collisions, interactions with the electrons of the valence band, of the core shells, collisions with the phonons). This has already been described elsewhere [9, 13–16].

In principle, this way of modelling the problem allows one to reproduce the experimental secondary-electron emission yield curve in a situation where the charge effects are negligible. In fact it has already been shown that the characteristics of the secondary emission curve is strongly influenced by the low-energy electron transport processes. In particular the transition from a free motion to a polaron state is essential for correctly accounting for the variation of the total secondary emission yield with the primary energy [17].

The present simulation results are compared with the known experimental values for SiO_2 targets [18–20] (figure 1). The agreement is gratifying, especially as our aim here is not to reproduce accurately the characteristics of the secondary emission of a given sample but rather to deduce general tendencies for the internal charge constitution. One notices that the cut-off energy E_{c2}, for which $\sigma = 1$, is located near 1600 eV.

The original characteristic of our model concerns the introduction of the polarization effects induced in the medium by the charges. At very low energies (typically under a few eV), a charge carrier (electron or hole) can significantly interact with the lattice by means

of electromechanical effects. From this, the particle, characterized by an increased effective mass, will drift along the internal electric field lines, surrounded by its 'polarization cloud' (polaron scheme) [21–24].

Depending on the materials, the coupling between a charge carrier and the polarization will be more or less important, leading to different localization radii for the polaron. The coupling parameter α introduced by Fröhlich [25] allows one to calibrate the intensity of these effects. The higher the value of α is, the stronger the interaction will be. In the case of electrons injected in an amorphous SiO_2 sample, one has $\alpha = 1.3$ [26]. So, the effects related to the interactions with the polarization field will remain rather weak. It follows that the mobility of the electron–polaron is high. If one refers to Hughes [26] or Fitting [27], a value of $\mu_e = 20$ cm^2 V^{-1} s^{-1} can be retained for the mobility.

For the holes, the situation is more complex. By reference to the results obtained by Hughes and Emin [28, 29], for amorphous SiO_2, several regimes can be distinguished. When it has just been created by pair excitation, a hole has a rather high mobility. In the following phase its mobility falls abruptly and can, according to Hughes and Emin [29], become of the order of 10^{-6} times that of an electron. This effect is commonly attributed to the formation of a small polaron [28, 29]. Finally, after the first trapping event, the hole moves slowly by hopping and exhibits a dispersive transport. In the present work, we have simply taken a 'compromise' value $\mu_h = 0.01$ cm^2 V^{-1} s^{-1} for the mean mobility of a hole to account for the first two phases in a global way.

The polarons can be stabilized when they encounter an empty trapping site. Charge trapping is indeed a complex problem which has been discussed by many authors (see for instance [30] or [31]). In particular, the nature of the traps may be quite varied (charged or neutral impurities, dislocations, grain boundaries, ...) and their concentration can differ considerably from one sample to the other. For instance, Cazaux [3] indicates the following values of trapping site densities for different kinds of material: $N_t \approx 10^{22}$ cm^{-3} for an amorphous sample, about 10^{16} cm^{-3} for a crystal with impurities and from 10^{17} to 10^{20} cm^{-3} for polycrystals.

In a polarizable medium, besides the influence of these traps, extrinsic by nature, one has to account for self-localization effects for the charge carriers which have formed polarons [15, 16]. The density of these intrinsic traps can be much higher, *a priori* of the order of the molecular density, typically 10^{22} sites cm^{-3}.

On account of the great diversity of the possible trapping sites and also due to the lack of proper scattering cross-sections for the interactions of the charge carriers with these traps, it is an essentially qualitative approach that has been retained for the present study. We have made the hypothesis that all the trapping effects can be characterized as a whole by a mean scattering cross-section [15, 16]. According to this description, as soon as a polaron penetrates into a given cell with available trapping sites, there is every chance that it stabilizes there.

The traps are supposed to be uniformly distributed in the volume of the target. They are assumed to be initially neutral, so that either electrons or holes can fix there.

Three situations can then occur. If the trapping site is empty, the polaron can fix. If it is occupied by a carrier of the same sign, an exclusion effect takes place. The polaron is not able to fix there and it drifts again by following the field lines. Finally, if the site is occupied by a carrier of opposite sign, the polaron recombines. The site is thus liberated and both charges leave the transport process.

In order to simplify the calculations, the possibility of electron or hole detrapping by the internal field has not been included in the present version of our model. In fact, we have supposed that the traps are sufficiently deep to ensure the stability of the charge distribution throughout the simulated experiment.

As already indicated, the charges accumulated in the target generate an electrostatic field which modifies the particle trajectories. Under this influence the charge distribution is itself modified, and so on, so the calculations have to be made self-consistently.

From a given charge distribution implanted in a uniform medium, it is possible to evaluate the potential anywhere by using Poisson's equation. This latter can be solved by using a finite-difference algorithm [32].

3. Simulations in the negative charge regime

As the charge of the insulator depends both on the characteristics of the target and on those of the primary beam, for the calculations presented here, we have tried to reproduce at best the conditions encountered in an electron microscopy experiment.

Concerning the primary beam, the intensities I usually selected for the primary current are of the order of 10^{-9}–10^{-10} A [33]. Here we have considered the case of a highly focused primary beam, with a spot diameter $d = 5$ nm at the surface of the sample. The irradiated surface is $S \approx 20$ nm^2 (i.e. 2×10^{-13} cm^2). The primary current density is then of the order of $j = 5 \times 10^2$ A cm^{-2}. The primary beam intensity is directly related to the time τ_p between two successive arrivals of electrons at the surface: $\tau_p = |e|/I$, where e represents the electron charge (10^{-19} C). By using a beam intensity of 10^{-9} A, one thus obtains $\tau_p = 0.1$ ns.

In order to lead to a negative charging regime, the kinetic energy E_p of the primary beam electrons has typically to be of a few keV ($E_p > E_{c2}$).

The parameters related to the target (density of traps, carrier mobility, ...) are intended to fit the case of amorphous SiO_2. However, we presume that the results that we have obtained have a much broader validity and are representative of what happens in most insulators.

For SiO_2, the atomic density is 3×10^{22} cm^{-3}. On account of the presence of both intrinsic and extrinsic trapping sites, we are led to use a mean trapping site density N_t of 10^{19} cm^{-3}, i.e. of a little more than one site per cubic cell of 5 nm side length.

3.1. General behaviour in the negative charge regime

A first study has been performed by using a primary beam energy $E_p = 2500$ eV—that is, a value close to the cut-off energy ($E_{c2} \approx 1600$ eV). The simulation makes use of a statistical sample of 10^8 primary electrons, which is equivalent to an injected dose of 16 pC and a total irradiation time of 10 ms. The injected dose is thus of the order of magnitude of that used during an electron microscopy experiment. The density of trapping sites for this first study has been fixed at $N_t = 1.6 \times 10^{19}$ cm^{-3}.

For the primary energy considered, the computed initial value of the total secondary-electron emission yield σ is close to 0.75 (see figure 1). During the bombardment, the electrical neutrality of the sample is destroyed, leading to an excess of negative charges in the sample. The surface potential in the impact zone of the primary beam, V_s, becomes more and more negative, resulting in a slowing down of the primary electrons before they penetrate into the sample. The effective energy of the beam at the point of impact is thus $E_{\text{eff}} = E_p + |e|V_s$, so the total secondary emission yield σ (which includes the true secondary electrons and the backscattered ones) increases during the bombardment (figure 2). Let us nevertheless remark that σ always remains lower than unity, which implies that the number of excess negative charges continuously increases (figure 3). Thus, the surface potential V_s itself decreases progressively (figure 4).

The evolution of the system goes on as long as the total secondary emission yield is still lower than unity (self-regulation of the yield). When σ reaches unity, the system is indeed

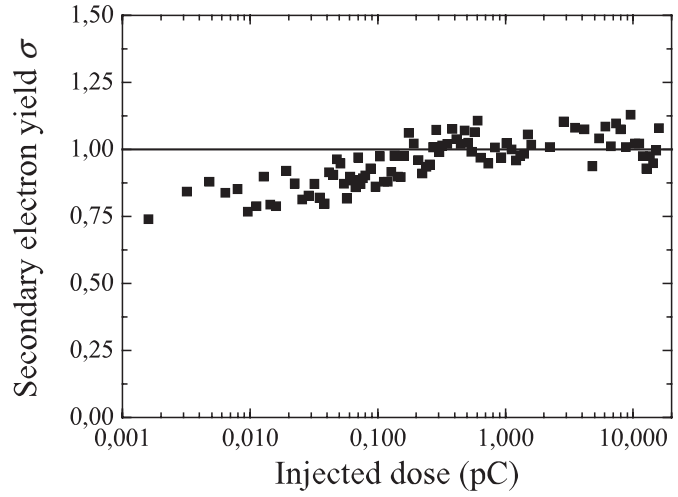

Figure 2. Evolution of the total secondary-electron emission yield σ as a function of the injected primary dose. The primary energy is $E_p = 2500$ eV and the density of trapping sites is $N_T = 1.6 \times 10^{19}$ cm^{-3}.

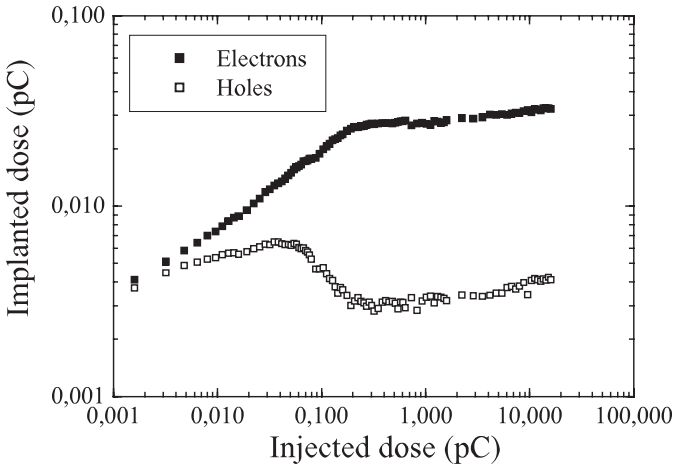

Figure 3. Evolution of the dose of trapped electrons and holes as a function of the injected primary dose. The primary energy is $E_p = 2500$ eV and the density of trapping sites is $N_T = 1.6 \times 10^{19}$ cm^{-3}.

globally in a stationary state: one secondary electron is emitted for each injected primary electron. As a consequence, the number of excess charges stabilizes to a practically constant value (figure 3), and V_s reaches a limit value, here close to -600 V (figure 4). In figures 2–4, one remarks that the quasi-stationary state is reached as soon as a dose of about 0.3 pC has been injected.

In this calculation, all the excess charges are fixed in traps. The number of itinerant polarons (electrons or holes) is practically zero throughout the simulation.

Figure 3 allows us to distinguish three steps in the building up of the charge. In the first step, until the injection of a primary dose of about 0.04 pC, the numbers of trapped electrons and holes regularly increase. In the second step, from 0.04 to about 0.3 pC, the number of

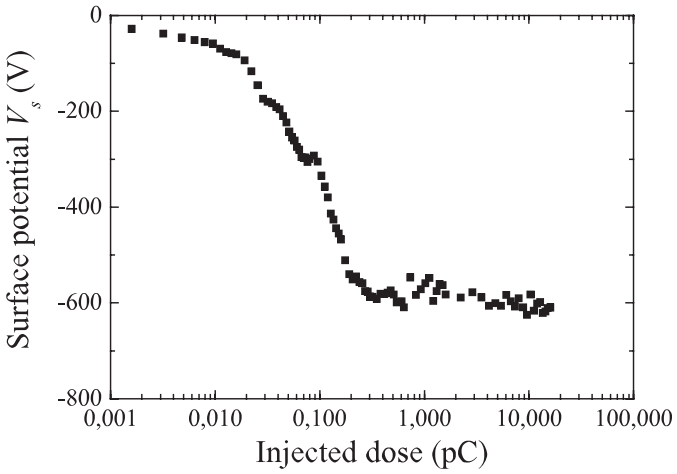

Figure 4. Evolution of the potential at the impact point V_s as a function of the injected primary dose. The primary energy is $E_p = 2500$ eV and the density of trapping sites is $N_T = 1.6 \times 10^{19}$ cm^{-3}.

trapped holes decreases rapidly. The electrons, however, continue to be trapped. After the injection of 0.3 pC, the quasi-stationary regime is reached and the numbers of positive and negative carriers getting fixed in traps increase very slowly.

Figure 5 enables us to understand the origin of this behaviour. The panels represent the evolution of the spatial distribution of the trapped charges during the bombardment. For readier comprehension, densities of trapped charges have been presented. The negative charge densities are shown in black, the positive ones in white. Moreover, they have been normalized to that of the trapping sites in order to make the saturated regions more apparent.

Figure 5(a) corresponds to the injection of 0.04 pC. It is thus representative of the first stage of the charge. In this state, two very distinct zones appear. The external region is populated by trapped negative charges. It has the shape of a 'shell', delimited by two axi-symmetrical half-ellipsoids elongated along the z-axis. It surrounds an internal zone, quite mixed and almost entirely populated by holes.

The half-lengths of the major axes (z-direction) are approximately $Z_1 = 180$ nm and $Z_2 = 220$ nm; those of the minor axes (ρ-direction) are about $R_1 = 100$ nm and $R_2 = 160$ nm. These values are quite comparable with the maximum penetration depth $Z_{\max}$ and the maximum lateral dispersion length $R_{\max}$ of the primary electrons. Figure 6, where the values taken by these two quantities as functions of the primary energy are reported, actually indicates that $Z_{\max} = 200$ nm and $R_{\max} = 160$ nm when $E_p = 2500$ eV.

In this first stage of the charge, the penetration is not much influenced by the diminution of the effective energy. The surface potential, after injection of 0.04 pC, is close to -200 V (figure 4). This corresponds to a reduction of $Z_{\max}$ and of $R_{\max}$ of about 20 nm, i.e. a relative reduction of 10%.

The trapping of the negative charges in the shell is made possible because very few holes can be found there. The slow negative carriers can reach regions more remote from the impact zone than the holes. These latter are trapped just at the excitation position of the pair and the recombination processes are practically non-existent in the shell periphery.

From the simulation, the mean density of negative charges in this zone can be estimated as 1.5×10^{19} cm^{-3}, which practically corresponds to the saturation of the trapping sites.

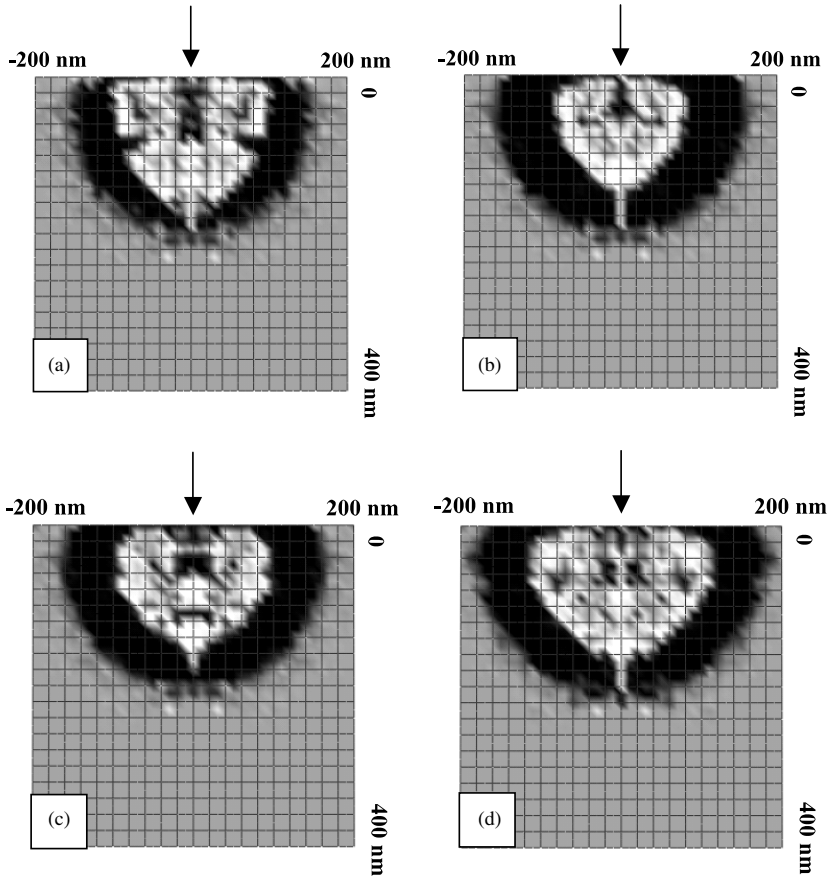

Figure 5. Trapped charge density for different injected primary doses: (a) 0.04 pC, (b) 0.3 pC, (c) 1 pC, (d) 10 pC. The primary energy is $E_p = 2500$ eV and the density of trapping sites is $N_T = 1.6 \times 10^{19}$ cm^{-3}. The negative charges are represented in black, the positive charges in white. The maximum intensity of the greyscale corresponds to N_T.

The central region is the mixing zone where the electron–hole pairs are produced. It determines, at any time, the internal limit of the negative shell. At 2500 eV, the number of excited pairs per primary electron is close to 100. A simple calculation of the order of magnitude shows that most of them recombine. For instance, about 4 pC of holes are excited after the injection of a 0.04 pC dose. However, only 0.006 pC of trapped holes are found to remain, which means a 0.15% rate.

The second phase of the charge is characterized by the elimination of trapped holes. As shown by figure 5(b), corresponding to the injection of 0.3 pC, it is the interior part of the negative charge shell that has principally grown. One finds $Z_1 = 140$ nm and $R_1 = 100$ nm. For this primary dose, the effective energy E_{eff} is about 1900 eV. The maximum penetration depth is then $Z_{\max} = 135$ nm and the maximum lateral dispersion length is $R_{\max} = 110$ nm. The volume of the mixing zone has thus progressively diminished and the electrons have gradually eliminated the holes at its periphery (see also figure 3).

Beyond the primary dose of 0.3 pC, the system is practically in a quasi-stationary state and the total implanted charge remains globally constant. Figures 5(c) and 5(d) represent the spatial distribution of the trapped charges after the injection of 1 and 10 pC respectively. For this last

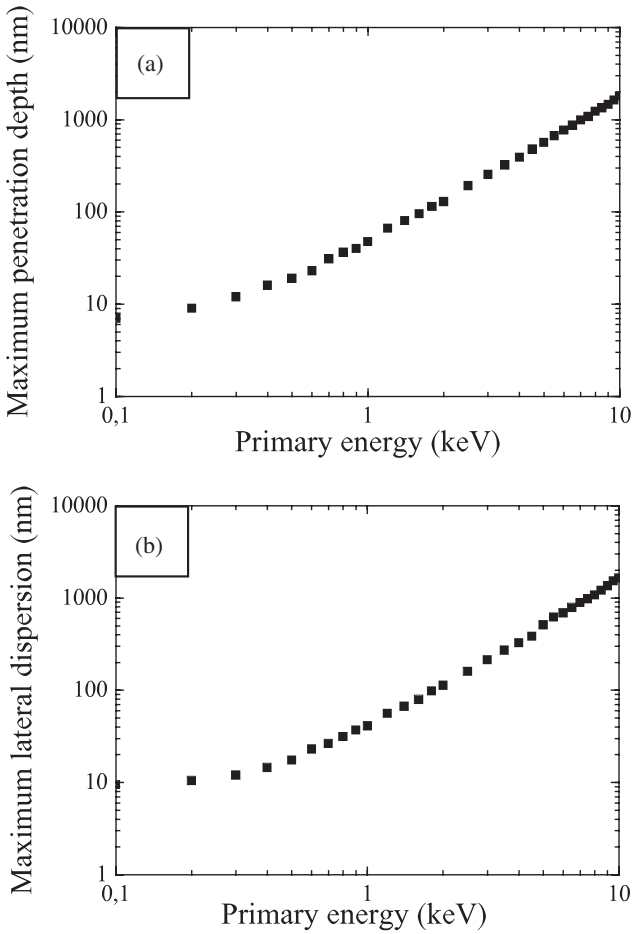

Figure 6. The maximum range of the primary electrons deduced from our simulations: (a) maximum penetration depth Z_{max}, (b) maximum lateral dispersion R_{max}.

phase of the charge, the effective energy is constant. The size of the mixing zone no longer changes. The primary electrons always tend to be trapped in the same region, escaping thus to possible recombination. This explains why the numbers of negative and positive carriers increase simultaneously.

One must not however forget that the capacity of a given region to accept trapped charges is limited by the density of traps of the material. So the negative shell will very quickly get saturated, as already shown in figure 5(c), and the primary electrons can no longer be trapped. They will have the choice of either being driven back to the mixing zone and recombining or migrating toward the exterior of the charged zone. This latter effect is confirmed by figure 5(d) where one observes that the negative shell actually spreads out. This phenomenon is however very slow and only the injection of a massive dose of primary electrons (10 pC) has permitted us to evidence it.

Finally, the external dimensions of the charged zone remain of the order of magnitude of the maximum penetration lengths Z_{max} and R_{max} (see figure 6). The volume of the negative shell is about 10^{-14} cm^3, leading to a mean density of negative charge of 2×10^{19} cm^{-3} in

Table 1. Characteristic parameters for the trapped charge at different primary energies.

E_p (eV)	Q_{Stab} (pC)	Q_{Trap} (pC)	σ_{init}	N_P	π	Q_e (pC)	Q_h (pC)	$R_{h/e}$ (%)
2 500	−0.32	−0.03	0.75	100	0.09	−0.032	0.004	12.5
5 000	−1.3	−0.23	0.5	200	0.18	−0.27	0.04	13.9
10 000	−4.0	−1.36	0.4	380	0.34	−1.7	0.34	19.8

this zone. Though it is necessarily overestimated, this value shows that the trapping sites are practically saturated in the negative shell. For the internal mixing zone, one can estimate that the mean density of trapped holes is of the order of 5×10^{18} cm^{-3}.

The charge balance itself shows that the dose of trapped electrons only represents a small part of the injected dose. At the beginning of the quasi-stationary regime, the trapping yield (number of trapped charges divided by the injected ones) is of the order of 10%. Of course it falls further for more important primary doses until it finally tends to zero. In this phase, the trapped holes only represent about 10% of the trapped electron number.

Let us recall that various electrostatic mirror experiments [34, 35] also suggest an 'in-shell' distribution of the implanted charges. This causes, after the vanishing of the mirror, the appearance of a ring of negative charges at the surface of the sample, surrounding a very weakly charged region. The mean diameter of the ring is of the order of magnitude of the primary electron penetration depth and the measured trapping abilities are quite comparable with what we obtain by simulation.

3.2. Influence of the primary energy

It is important to know whether the general behaviour described above is also operative for all the primary energies in the negative charge domain. For this we have simulated the bombardment of the same amorphous SiO_2 target for $E_p = 5000$ and 10 000 eV, the other parameters of the simulation remaining unchanged.

Figures 7(a) and 7(b) respectively present the evolution of the number of trapped electrons and that of the number of trapped holes during the bombardment for the three primary energies retained here. The three charge phases detailed in the preceding paragraph are found again in each case. In order to make the interpretation of the curves easier, some important quantities have also been collected in table 1.

For each simulation that we present, the self-regulation of the yield occurs and the system attains a quasi-stationary regime after injection of a primary dose Q_{Stab}. This dose is all the more important as the initial energy E_p of the beam is high. This is a consequence of the variation of the penetration depth of the primary electrons [36], which is more pronounced at high energies (figure 6(a)).

When the quasi-stationary regime is reached, the total trapped dose Q_{Trap} also increases with E_p. It represents about 9% of the injected dose at 2500 eV, 18% at 5000 eV and 34% at 10 000 eV. One could think that this is simply the result of changing the initial value of the total secondary emission yield σ_{init}. However, one easily understands, by referring to table 1, that this variation is not sufficient to explain the observed evolution. On the other hand, one observes in the same table that the proportion N_p of the electron–hole pairs excited per primary electron varies practically linearly with E_p in the energy range that we are concerned with. This explains the above-mentioned increase of the trapped dose. One also notices that the charging capacity $\pi = Q_{\text{Trap}}/Q_{\text{Stab}}$ is, for all the primary energies considered, constantly inversely proportional to N_p. So, the trapping yield π, as soon as the system becomes stabilized, is given, in a first approximation, by a law of the type $\pi = AE_p$, with $A \approx 3.5 \times 10^{-2}$ keV^{-1}.

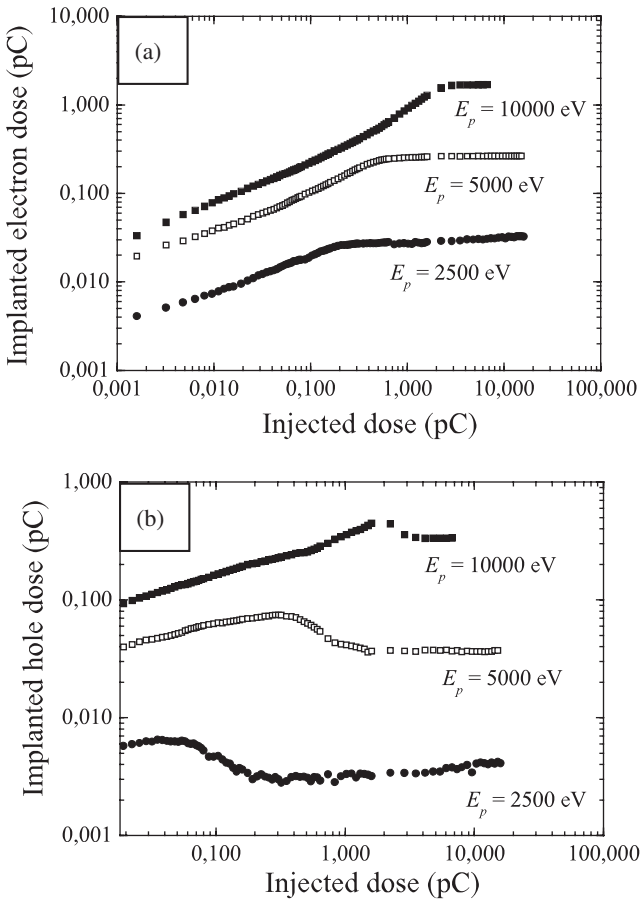

Figure 7. Evolution of the implanted dose as a function of the injected dose for different primary energies E_P. (a) Electrons, (b) holes.

This is only valid if the recombination rate remains constant at each primary energy. In all the cases that we have investigated here, the trapped hole dose Q_h remains much lower than that of the trapped electrons Q_e (table 1). At 2500 eV, the proportion of the two types of population, $R_{h/e}$, is of the order of 12%. It reaches 14% at 5000 eV and 20% at 10 000 eV, showing a non-negligible dependence of the recombination rate on E_p. However, on account of the small fraction of trapped holes compared to the electrons, the recombination plays only a secondary role.

The panels of figure 8 show the charge distributions in the quasi-stationary state for primary energies of 5000 eV (a) and 10 000 eV (b). The characteristic 'in-shell' shape is present in both cases and the external dimensions are always of the order of the maximum penetration depth and of the maximum lateral dispersion of the primary beam. We actually obtain $Z_2 = 550$ nm and $R_2 = 480$ nm for a $Z_{\max}$ of 570 nm and an $R_{\max}$ of 510 nm at 5000 eV. At 10 000 eV, these values become $Z_2 = 1650$ nm, $R_2 = 1300$ nm, $Z_{\max} = 1800$ nm and $R_{\max} = 1650$ nm. Let us however remark that, on account of the contrasts used in figure 8, the values of Z_2 and R_2 are difficult to estimate.

The internal delimitation of the negative shell is much less sharp than in the $E_p = 2500$ eV case. In fact, the slowing down of the primary beam is all the more marked as the primary energy is high. In the case of a bombardment at 5000 eV, the effective energy of the beam E_{eff}

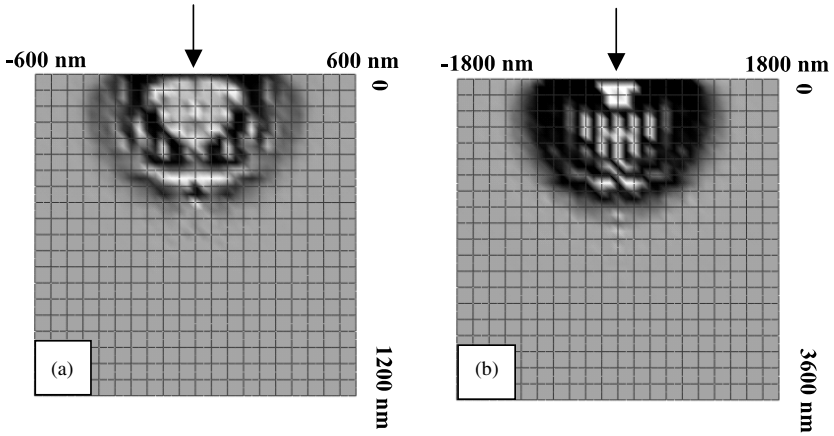

Figure 8. Densities of trapped charges for different primary energies. (a) $E_p = 5000$ eV, (b) $E_p = 10\,000$ eV. In both cases the maximum intensity of the greyscale corresponds to $N_T = 1.6 \times 10^{19}$ cm^{-3}. The charge states indicated are representative of a system in which the quasi-stationary regime has been reached. This corresponds to an injected primary dose of: (a) 2 pC, (b) 4 pC.

falls to 2600 eV at the end of the charging. The maximum penetration of the electrons decreases from $Z_{\max} = 570$ nm to a final value of 205 nm. The same holds for $R_{\max}$. For a bombardment at 10 000 eV, $Z_{\max}$ goes from 1800 to 250 nm! In these conditions, the negatively charged region is now disseminated over an important thickness, nearly 1500 nm at $E_p = 10\,000$ eV. Let us finally remark that the negative shell is no longer uniformly charged as in the case of a primary energy of 2500 eV. The slowing down takes place too rapidly and the primary electrons cannot annihilate all the holes present there to uniformly fill the zones concerned.

3.3. Influence of the density of trapping sites

We have carried out simulations for a primary energy $E_p = 2500$ eV, for different trapping site densities N_T. The values retained were 1.6×10^{18}, 1.6×10^{19} and 1.6×10^{20} cm^{-3}. This corresponds respectively to one trapping site in a volume of 625×10^3, 625×10^2 and 625×10^1 Å^3, which represents approximately one site per 5×10^3, 5×10^2 and 5×10^1 SiO_2 molecules.

The simulations were continued until the quasi-stationary regime was attained, except for the case of $N_T = 1.6 \times 10^{18}$ cm^{-3}. In this latter situation, the calculations become excessively long as soon as the injected dose reaches 0.03 pC. We will try to determine the origin of this limitation in what follows.

For the two highest densities of sites, the regulation of the yield occurs correctly. The quasi-stationary state is attained for injected doses which are very similar in the two cases, i.e. about 0.3 pC. On account of the low value of the injected dose, the regulation is just beginning in the case $N_T = 1.6 \times 10^{18}$ cm^{-3}.

In figures 9(a) and 9(b), we have reported the evolution of the doses of trapped electrons and of trapped holes during the charging. The three charge phases are always present for high densities of trapping sites. The implanted doses stabilize at limit values which, quite logically, grow with increasing N_T. The total implanted dose Q_{Trap} is -0.035 pC when $N_T = 1.6 \times 10^{20}$ cm^{-3}, whereas it is -0.028 pC in the case where $N_T = 1.6 \times 10^{19}$ cm^{-3}.

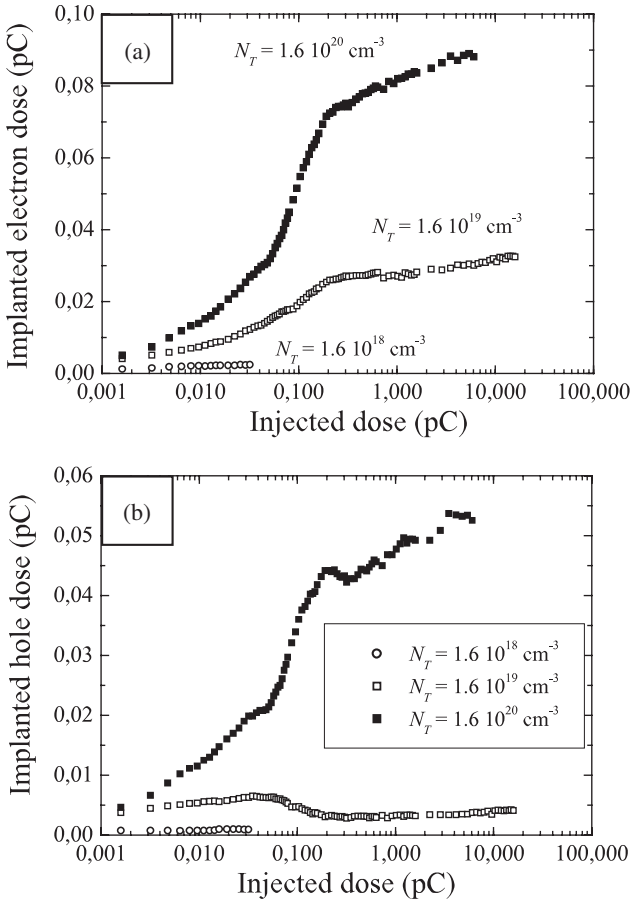

Figure 9. Evolution of the implanted dose as a function of the injected dose for different densities of trapping sites N_T. (a) Electrons, (b) holes. The primary energy is $E_p = 2500$ eV.

The dependence of Q_{Trap} on N_T is however difficult to determine from these two examples. Let us also remark that in the case of $N_T = 1.6 \times 10^{20}$ cm^{-3}, the numbers of trapped electrons and holes always increase in the third charge regime. The global charge remains nevertheless constant. We will see hereafter that in this situation the traps are far from being saturated.

The balance of the trapped charges also varies with N_T. The ratio of the trapped populations for the two types of carrier reduces when the density of sites increases. While it attains 1 against 10 in favour of the electrons for $N_T = 1.6 \times 10^{18}$ cm^{-3}, it falls to 1 against 6 for $N_T = 1.6 \times 10^{19}$ cm^{-3} and to 2 against 3 for $N_T = 1.6 \times 10^{20}$ cm^{-3}. This can be explained by the fact that the recombination processes play a leading role when the number of places available for trapping decreases.

In all the cases that we have studied up to now, the number of itinerant polarons (electrons and holes) was always approximately zero throughout the charging. The situation is however quite different for the low trapping site densities ($N_T = 1.8 \times 10^{18}$ cm^{-3}). Study of figure 10, which shows the evolution of the number of itinerant carriers during the simulation, is particularly instructive. It appears indeed that the electrons in that case encounter more and more difficulty in getting trapped. First, the number of negative carriers is limited by the recombination with itinerant holes. These latter disappear progressively and their number

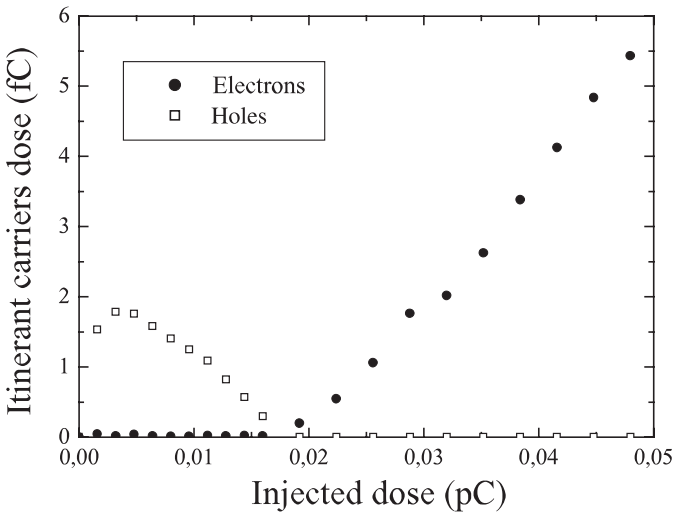

Figure 10. Evolution of the number of itinerant carriers during the simulation. The primary energy is $E_p = 2500$ eV and the density of trapping sites is $N_T = 1.6 \times 10^{18}$ cm^{-3}.

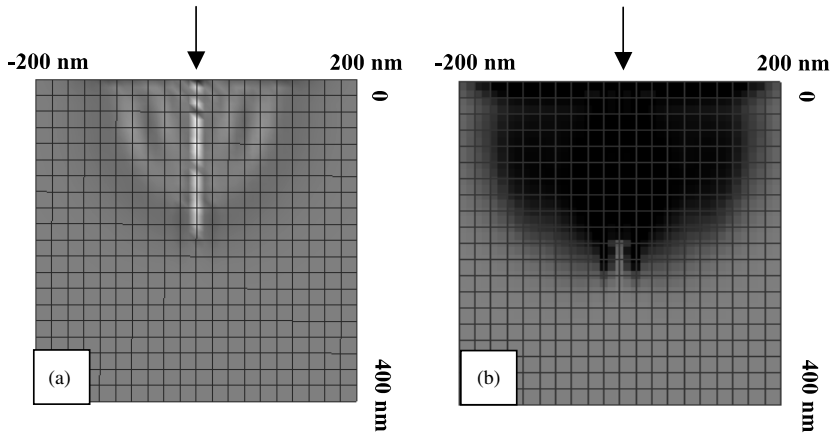

Figure 11. Densities of trapped charges for different densities of trapping sites. (a) $N_T = 1.6 \times 10^{20}$ cm^{-3}, (b) $N_T = 1.6 \times 10^{18}$ cm^{-3}. The primary energy is $E_p = 2500$ eV. The maximum intensity of the greyscale corresponds to N_T.

remains practically zero as soon as the injection attains 0.02 pC. The proportion of itinerant electrons then begins to increase. This phenomenon is obviously related to the saturation of the traps.

Figure 11(a) accounts for the charge state in the quasi-stationary regime, for $N_T = 1.6 \times 10^{20}$ cm^{-3} (see figure 5(b) for the case of $N_T = 1.6 \times 10^{19}$ cm^{-3}). The external dimensions are still given by the maximum penetration of the primary electrons.

When the density of trapping sites is high ($N_T = 1.6 \times 10^{20}$ cm^{-3}), at this stage of the injection, the traps are still weakly occupied (figure 11(a)). The calculations indicate that the maximum density of occupation is obtained under the impact zone, with a value close to 0.8 N_T. In the negative shell, the density of trapped electrons is only of the order of 1.9×10^{19} cm^{-3}. With reference to its dimensions, one can roughly estimate the volume of

the wall to be 7.8×10^9 Å^3. By using the total number of trapped charges given by figure 9, one would obtain a density of trapped electrons close to 2.4×10^{19} cm^{-3} if all of them were located in the wall, a value not too far from the above one.

The next figure 11(b) corresponds to $N_T = 1.6 \times 10^{18}$ cm^{-3}. The maximum dimensions of the charged zone remain of the same order as the penetration distance of the primary electrons. One notices that not only is the charged region saturated, but also the whole mixing zone is now occupied by trapped electrons. The volume estimated for this zone is about 1.1×10^{10} Å^3. The maximum number of carriers that can get trapped there is then 1.8×10^4. However, figure 9 indicates that the total trapped charge is about 0.03 pC, i.e. 1.9×10^4 electrons. This shows that no more room is available as soon as this dose has been implanted.

In this system state, the electrons that issued from the cascade remain captive in the mixing zone. The electric field produced by the carriers that have already fixed prevents them from reaching neutral external regions. They can still recombine with the holes, itinerant or trapped. However, on account of a total secondary emission yield lower than unity, the positive carriers are always in a smaller proportion than the negative ones and they are progressively eliminated. Then, the number of itinerant electrons never stops increasing (figure 10), causing extreme slowing down of the simulation development. In this latter case, the maximum dose of trapped electrons is no longer limited by the self-regulation of the total secondary emission yield, but is now limited by the density of trapping sites.

Let us also remark that this confining situation takes much longer to attain for higher primary energies, this effect being accompanied by an increase of the maximum dose that can be trapped.

4. Conclusions

In the present work, we have simulated the implantation of a negative charge by an electron beam in an insulating target. The theoretical electron–insulator interaction model formerly developed by us was used for this. The parameters retained for these calculations (injected dose, primary beam energy) account for situations quite comparable with those encountered in electron microscopy experiments.

We were particularly interested in the charge distribution produced by a fixed and well-focused electron beam. In all the cases studied here, a semi-ellipsoidal negative shell builds up, surrounding a mixing zone with a weak density of positive charge. Three different phases appear in the building up of the charge.

The first step corresponds to the emergence of the negative shell. Its shape is obviously governed by the penetration of the primary beam and by its progressive straggling in the sample. This behaviour is common to all (homogeneous) materials but the actual size of this zone depends on the interaction cross-sections appropriate to the medium studied. As already indicated above, some simple empirical range–energy relations can be used to relate for instance the penetration of the primary beam to the atomic number of the target. The consequence of the formation of the shell is that an electrostatic field builds up which acts as a barrier for negative carriers, which also favours their recombination with the positive charges. The itinerant charge carriers are thus confined to the internal zone delimited by the negative shell.

Globally, the thickness of the shell increases along with the magnitude of the field, so the penetration of the primary beam into the interaction zone is progressively reduced. This reduction of the effective energy characterizes the second phase. The rate at which the thickness of the shell grows is governed by the dynamics of the recombination and trapping processes, which can differ substantially from one sample to the other (see [37, 38] for instance). Several other physical parameters (dielectric constant, structure defects, nature and density of trapping

sites, electron and hole mobilities, recombination times for electrons and holes, material modification by irradiation, ...) will cause differences. This is obviously a huge problem which could not be approached in the present context, where the attention was solely focused on the role of the trap density.

The third phase corresponds to the stabilization of the charge, due to the self-regulation of the secondary emission. In the negative charging regime, this regulation occurs when the effective energy of the primary beam has increased to a value close to the cut-off value E_{c2} and the total secondary yield is equal to unity [39]. The dynamics of this process depends on the sample characteristics. For instance, the final surface potential practically equals $E_p - E_{c2}$ and SiO_2 ($E_{c2} \sim 1600$ eV [18–20]), in this respect, is quite different to MgO ($E_{c2} \sim 27$ keV [15]) and to Al_2O_3 ($E_{c2} \sim 8$ keV [15]). In the stabilization phase, the density of trapping sites also plays a central role. For instance, in the case where this density is weak, the sites are rapidly saturated and the total secondary emission yield never reaches unity. Our simulation does not permit us to follow the charge evolution any longer.

The results that we have presented apply well to the case where the activation energies of the traps are high. A next step in our work is including the possibility of charge detrapping processes and simulating situations where the relaxation effects can play a significant role.

The present calculations have to be seen in the more general framework of the characterization of insulating materials. Up to now, the experimental techniques, such as the scanning electron microscope mirror method (SEMM), have given interesting information on the potential distribution generated by an implanted charge. However, the inverse problem, which consists in deducing the charge distribution from the potential, is much more difficult, as the solution is generally not unique. Our simulations of charge implantation, based on physical arguments, can be used to build models in order to estimate the charge distribution extent and also for instance the density of traps.

Acknowledgment

Most of this work was performed with the financial support of the French 'Commissariat à l'Energie Atomique' (CEA/DAM). The authors would like thank this institution for its help.

References

[1] Dissado L A and Forthergill J C 1992 *Electrical Degradation and Breakdown in Polymers* (London: Peregrinus for IEE)
[2] Le Gressus C 1998 *Le Vide: Science, Technique et Applications (Suppl.)* **287** 733
[3] Cazaux J 1996 *X-Ray Spectrom.* **25** 265
[4] Blaise G and Le Gressus C 1991 *J. Appl. Phys.* **69** 6334
[5] Stoneham A M 1998 *Le Vide: Science, Technique et Applications (Suppl.)* **287** 1
[6] Damamme G, Le Gressus C and DeReggi A S 1997 *IEEE Trans. Dielectr. Electr. Insul.* **4** 558
[7] Kotera M and Suga H 1988 *J. Appl. Phys.* **63** 261
[8] Vicario E, Rosenberg N and Renoud R 1994 *Surf. Int. Anal.* **22** 115
[9] Renoud R 1995 *Thèse de Doctorat* Université Lyon I
[10] Di Fabrizio E, Grella L, Baciocchi M, Gentili M, Ascoli C, Cappella B, Frediani C and Morales P 1997 *J. Vac. Sci. Technol.* B **15** 2892
[11] Hwu J J, Ko Y-U and Joy D C 2000 *Proc. SPIE* **3998** 239
[12] Jbara O, Portron B, Mouze D and Cazaux J 1997 *X-Ray Spectrom.* **26** 291
[13] Ganachaud J-P, Attard C and Renoud R 1997 *Phys. Status Solidi* b **199** 175
[14] Attard C and Ganachaud J-P 1997 *Phys. Status Solidi* b **199** 455
[15] Attard C 1998 *Thèse de Doctorat* Université de Nantes
[16] Renoud R, Attard C, Ganachaud J-P, Bartholomé S and Dubus A 1998 *J. Phys.: Condens. Matter* **10** 5821
[17] Ganachaud J-P and Mokrani A 1995 *Surf. Sci.* **334** 329

[18] Dionne G F 1975 *J. Appl. Phys.* **46** 3347
[19] Joy D C and Joy C S 1995 *SEMATECH Report*
[20] Whetten N R (ed) 1962 *Methods in Experimental Physics* vol 4 (New York: Academic)
[21] Austin I G and Mott N F 1969 *Adv. Phys.* **18** 41
[22] Blaise G and Le Gressus C 1991 *J. Appl. Phys.* **69** 6334
[23] Blaise G 1992 *Le Vide, Les Couches Minces (Suppl.)* **260** 417
[24] Shluger A L and Stoneham A M 1993 *J. Phys.: Condens. Matter* **5** 3049
[25] Fröhlich H 1954 *Adv. Phys.* **3** 325
[26] Hughes R C 1975 *Phys. Rev. Lett.* **35** 449
[27] Fitting H-J 1993 *J. Vac. Sci. Technol.* B **11** 433
[28] Hughes R C 1977 *Phys. Rev.* B **15** 2012
[29] Hughes R C and Emin D 1978 The Physics of SiO_2 and its interfaces *Proc. Int. Topical Conf. on Physics of SiO_2 and its Interfaces* ed S T Pantelides (New York: Pergamon) p 14
[30] Stoneham A M 1975 Theory of defects in solids *Electronic Structure of Defects in Insulators and Semiconductors (Monographs on the Physics and Chemistry of Materials)* ed H Fröhlich, A J Heeger, P B Hirsch and N F Mott (Oxford: Clarendon)
[31] Buchanan D A, Fischetti M V and DiMaria D J 1991 *Phys. Rev.* B **43** 1471
[32] Durant E (ed) 1964 *Electrostatique. II—Problèmes Généraux. Conducteurs* (Paris: Masson)
[33] Reimer L 1985 Scanning electron microscopy *Physics of Image Formation and Microanalysis (Springer Series in Optical Sciences)* ed P W Hawkes (Berlin: Springer)
[34] Attard C, Bigarré J and Hourquebie P 2000 *Proc. 2nd Conf. on Electrostatics (Montpellier, France)* p 77
[35] Bigarré J, Attard C and Hourquebie P 2001 *Proc. CSC4: 4th Int. Conf. on Electric Charge in Non-Conductive Materials (Tours, France)* p 45
[36] Renoud R, Ganachaud J-P and Mady F 2001 *Proc. CSC4: 4th Int. Conf. on Electric Charge in Non-Conductive Materials (Tours, France)* p 376
[37] Martin P, Guizard S, Daguzan Ph, Petite G, D'Oliveira P, Meynadier P and Perdrix M 1997 *Phys. Rev.* B **55** 5799
[38] Guizard S, Martin P, Daguzan Ph, Petite G, Audebert P, Geindre J P, Dos Santos A and Antonnetti A 1995 *Europhys. Lett.* **29** 401
[39] Blaise G 2001 *Proc. CSC4: 4th Int. Conf. on Electric Charge in Non-Conductive Materials (Tours, France)* p 31